Optically Detected Structural Change in the N-Terminal Region of the Voltage-Sensor Domain

Hidekazu Tsutsui,[†‡*] Yuka Jinno,[†] Akiko Tomita,[†] and Yasushi Okamura[†]
[†]Laboratory of Integrative Physiology, Graduate School of Medicine, Osaka University, Osaka, Japan; and [‡]Formation of and Information Processing by Neural Networks, and Control, PRESTO, Japan Science and Technology Agency, Saitama, Japan

ABSTRACT The voltage-sensor domain (VSD) is a functional module that undergoes structural transitions in response to membrane potential changes and regulates its effectors, thereby playing a crucial role in amplifying and decoding membrane electrical signals. Ion-conductive pore and phosphoinositide phosphatase are the downstream effectors of voltage-gated channels and the voltage-sensing phosphatase, respectively. It is known that upon transition, the VSD generally acts on the region C-terminal to S4. However, whether the VSD also induces any structural changes in the N-terminal region of S1 has not been addressed directly. Here, we report the existence of such an N-terminal effect. We used two distinct optical reporters—one based on the Förster resonance energy transfer between a pair of fluorescent proteins, and the other based on fluorophore-labeled HaloTag—and studied the behavior of these reporters placed at the N-terminal end of the monomeric VSD derived from voltage-sensing phosphatase. We found that both of these reporters were affected by the VSD transition, generating voltage-dependent fluorescence readouts. We also observed that whereas the voltage dependencies of the N- and C-terminal effects appear to be tightly coupled, the local structural rearrangements reflect the way in which the VSD is loaded, demonstrating the flexible nature of the VSD.

INTRODUCTION

Membrane electrical signals occur and propagate rapidly, and play essential roles in a variety of physiological functions including secretion, muscle contraction, and neural transmission (1). These electrical signals are amplified and/or decoded by membrane proteins that use a conserved module, the voltage-sensor domain (VSD), to sense the transmembrane electric field. The VSD consists of four membrane-spanning segments (S1–S4) and undergoes a conformational transition from a down state at hyperpolarized voltages to an up state at depolarized voltages. The transition is coupled to effector function. In voltage-gated channels, the VSD is coupled to the gating of an ion-conductive pore consisting of four units of the S5-S6 segments (1), whereas in the voltage-sensing phosphatase (VSP), the effector is a monomeric phosphoinositide phosphatase whose enzymatic activity is regulated in a voltage-dependent manner (2). In the primary structures, the effectors of VSDs are typically located in the region C-terminal to S4.

Since the first molecular identification of a voltage-gated channel (3), efforts have been made to understand the transition mechanisms. Although atomic-scale structural information about each state would provide crucial clues, all of the VSD protein crystal structures resolved thus far likely reflect the up state (4–7). Nevertheless, a variety of approaches have shown that the transition at least involves the upward motion (i.e., from inside of the cell to outside) of S4 (8–14), even though the details of the transition mechanisms remain unresolved (15,16).

Along with this structural and functional evidence, it is generally accepted that the VSD acts on the region C-terminal to S4 upon its transition. In the conventional model for voltage-gated channels, for example, the covalent S4-S5 linker is thought to transmit force generated by S4 to the pore, thereby regulating its gating (17,18). Moreover, it has been shown that the VSD can be coupled to nonintrinsic effectors placed at the C-terminal end of S4, such as the pore domain of the other channel, as well as fluorescence reporters (19–21). In contrast to downstream actions of the VSD that occur C-terminally upon transition, whether the VSD transition also structurally affects the region N-terminal to S1 has not been directly addressed. Here, by taking advantage of the monomeric nature of the VSP-derived VSD, we were able to functionally introduce two different optical reporters into the N-terminal end of S1, which enabled us to detect the existence of such an upstream effect.

MATERIALS AND METHODS

Molecular biology

Site-directed mutagenesis was performed as described previously (22). Details of the constructs used in this study are described in Fig. S1 in the Supporting Material.

Electrophysiology and photometry in *Xenopus* oocytes

Xenopus oocyte preparation and the synthesis and microinjection of complementary RNAs (cRNAs) were performed as described previously (23,24). Simultaneous two-electrode voltage clamp (TEVC) and photometry were

Submitted March 22, 2013, and accepted for publication May 31, 2013.
*Correspondence: tsutsui@phys2.med.osaka-u.ac.jp
Editor: Chris Lingle.

0006-3495/13/07/0108/8 $2.00
http://dx.doi.org/10.1016/j.bpj.2013.05.051

performed using an amplifier (OC-725C; Warner Instruments, Hamden, CT) and an inverted microscope (IX70; Olympus, Tokyo, Japan) equipped with a stable 75 W xenon lamp (Ushio, Tokyo, Japan). Intracellular glass microelectrodes were filled with 2.5 M KCl (pH 7.2), and these had resistances ranging from 0.1 to 3.0 MΩ. A 20× objective lens (NA 0.70; Olympus) was used to collect fluorescence. The fluorescence emission spectrum from a voltage-clamped cell was acquired by delivering fluorescence output to a spectrophotometer (USB4000; Ocean Optics, Dunedin, FL) via an optical fiber (QP600-2-UV-VIS; Ocean Photonics). One or two photomultiplier (PMT) modules (H5784-02; Hamamatsu Photonics, Hamamatsu, Japan) were used for single- or dual-channel photometry, respectively. The outputs from PMT modules and the TEVC amplifier were digitized and stored using an A/D converter (1322A; Axon Instruments, Sunnyvale, CA) and pClamp8 software (Axon Instruments). For dual-channel photometry in Förster resonance energy transfer (FRET) experiments, fluorescence output at the IX70 side-port was further split using a dichroic mirror, band-pass filtered, and delivered to the donor and acceptor channel PMT modules. To label the HaloTag domain with tetramethylrhodamine (TMR)-conjugated ligand (Promega, Madison, WI), cRNA-injected oocytes were incubated for 15–30 min at 18°C with the ligand (final concentration of 2 μM) in ND96 solution with gentle agitation using a rotator (RT-30; Taitec, Tokyo, Japan). Cysteine labeling with thiol-reactive TMR-maleimide (Molecular Probes, Carlsbad, cA) was performed as described elsewhere (25). Data were averaged for four to six sweeps to reduce noise in TMR photometry, but not in FRET measurements. Gating currents (i.e., capacitive currents added by the motion of the electrically charged VSD) were measured using the conventional P/5 protocol. Data were analyzed using Clampfit (Axon Instruments) software. The scheme for the recording setup and the optical filters used are described in Fig. S2.

RESULTS

N-terminal effect detected using a FRET reporter

We obtained the first evidence (to our knowledge) for the existence of an N-terminal effect using a construct in which mUKG and mKOκ were placed in tandem at the N-terminal end of S1 (Fig. 1 *A*). mUKG and mKOκ are monomeric green- and orange-emitting fluorescent proteins that serve as the FRET donor and acceptor, respectively (21). The VSD contained a R217Q mutation to shift its voltage sensitivity into the hyperpolarized range (20,26), which was advantageous for characterizing gating charge movements with negligible superimposition of endogenous ionic currents in *Xenopus* oocytes. The construct showed fine membrane expression in oocytes, which were then used for simultaneous voltage-clamp and photometry. Although

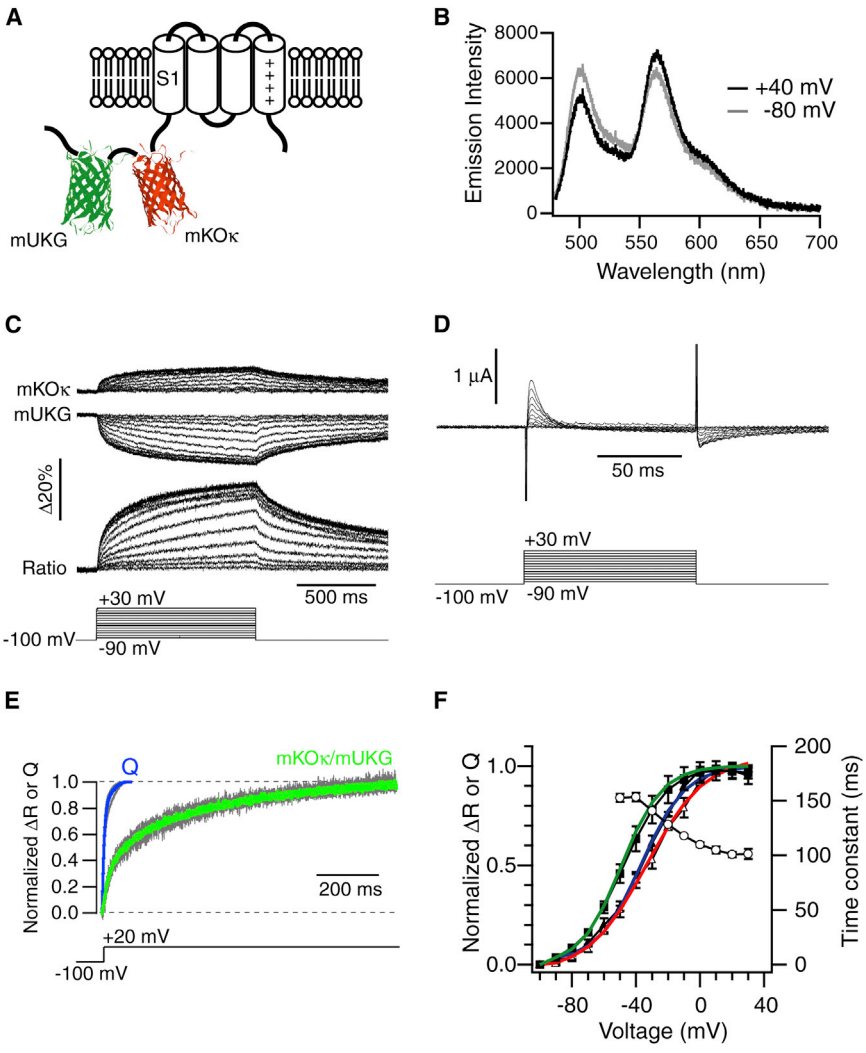

FIGURE 1 Optical signals from a FRET reporter at the N-terminal end of S1. (*A*) mUKG/mKOκ as a FRET pair at the N-terminal end of S1. (*B*) Emission spectrum from a voltage-clamped oocyte. The emission peaks for mUKG and mKOκ were 499 nm and 563 nm, respectively. (*C*) Changes in mUKG and mKOκ channel intensities and their ratio (mKOκ/mUKG) in response to voltage steps. (*D*) Representative traces for gating currents. (*E*) Comparison of the time course of gating charge movement (Q) and ratio signal (ΔR) in response to voltage step from −100 mV to +20 mV. Responses from four cells and their average are superimposed. In the online version, the averaged traces for Q and ΔR are highlighted in blue and green, respectively. (*F*) Voltage dependence of ΔR (*solid squares*; *solid line* = single Boltzmann's fit, Vmid = −49 mV, Zd = 1.9), activation time constants (*open circles*), and on (*solid triangles*; *solid line* = fit, Vmid = −36 mV, Zd = 1.8) and off (*open triangles*; *solid line* = fit, Vmid = −33 mV, Zd = 1.4) net gating charge movements (n = 4 cells). Error bars indicate SDs. In the online version, the curve fits for ΔR, Q-on, and Q-off are highlighted in green, blue, and red, respectively.

it was not expected initially, the donor and acceptor fluorescence exhibited clear reciprocal changes in response to switching the membrane voltage between –80 mV and +40 mV (Fig. 1 *B*). Upon depolarization, the acceptor/donor ratio increased by 33% ± 2.9% (mean ± SD; $n = 4$), which is comparable to the ratio change (~40%) achieved with the same FRET reporter placed at the C-terminal end of S4 (21). Next, we measured the time-resolved FRET response (Fig. 1 *C*), which showed slow kinetics compared with the gating charge movements (Fig. 1, *D* and *E*). The slow kinetics observed in the FRET response may indicate that the rearrangement within the FRET pair occurs slowly and is rate limiting. An alternative possibility is that the structural change at the N-terminus occurs as a secondary process and does not accompany robust charge movements. We next compared the steady-state responses. The voltage dependence of the ratio change correlated well with the net movement of the gating charge (Fig. 1 *F*). There was a small difference in the voltage dependence (Fig. 1 *F*), which would not be expected if a pure two-state model is assumed. However, the difference is not unreasonable, because the VSD, whether it originates from a channel or voltage-sensing phosphatase, has been shown to undergo multistep rearrangements (25,26). Presumably, the difference results simply from the nonlinearity of FRET readouts in detecting structural changes.

These observations clearly suggested that the VSD transition triggered structural changes at the N-terminus that affected the distance and/or orientation between the FRET donor and acceptor. However, there still remained the possibility that the phenomenon is only specific to the FRET reporter used. We therefore sought to evaluate the N-terminal effect using another approach.

N-terminal effect detected using a TMR-HaloTag

In fluorescent proteins, the fluorophores are buried within the β-barrel folds and are generally less sensitive to the environment than are organic small-molecule fluorophores (27). Therefore, we focused on the combination of an organic fluorophore, tetramethylrhodamine (TMR), and the second-generation haloalkane dehalogenase mutant (HaloTag7). TMR fluorescence is sensitive to local environmental factors, such as polarity (27), which has been employed to probe environmental changes around externally accessible cysteine residues (25,28). HaloTag7 is a soluble 33 kDa protein domain that can be specifically and covalently labeled with a variety of ligands (29). It is thought that upon specific labeling with a membrane-permeable TMR-conjugated ligand, the TMR fluorophore is positioned at the surface of HaloTag (30). We therefore hypothesized that the TMR-HaloTag could be used as a genetically encoded fluorescent reporter for environmental changes that can be tagged even cytoplasmically. Our idea was that the VSD could move the TMR-HaloTag at the cytoplasm-membrane interface, enabling observation of the resultant fluorescence change.

We first tested this idea using the C-terminal effect. HaloTag was placed downstream of S4 and labeled with a TMR ligand (Fig. 2 *A*). In response to depolarization, TMR exhibited a fluorescence decrease (Fig. 2 *B*). When a similar experiment was performed using the D129R mutant, in which proper membrane expression occurs but the voltage-dependent motion of S4 is ablated (31), TMR responses were completely abolished (Fig. 2 *C*). These data confirmed that the observed optical responses (Fig. 2 *B*) were not direct effects of the membrane potential change, but rather were dependent on the VSD transition. The voltage dependence of the steady-state fluorescence changes (ΔF) was well fit by a single Boltzmann function, and a clear voltage dependency was found in its kinetics (Fig. 2 *D*). We thus confirmed that the TMR-HaloTag is capable of reporting structural perturbations induced by the VSD transition. Importantly, the molecular mass of HaloTag (~33 kDa) is nearly twice as large as the S1–S4 segments combined (~17 kDa) and is similar to that of the phosphatase domain in VSP (~35 kDa (2)). Therefore, this result confirms the ability of VSD to drive an artificial effector with a substantial molecular mass.

Next, HaloTag was used to tag the N-terminal end of S1 (Fig. 2 *E*). Upon membrane depolarization, the original form exhibited a fluorescence decrease (Fig. 2 *F*), but the D129R mutant did not (Fig. 2 *G*). This again reveals the N-terminal effect of VSD transition. ΔF was in the same direction as the S4 signal (i.e., decreased fluorescence) and was comparable in amplitude (Fig. 2, *F* and *H*). We found that steady-state ΔF was well fit by a single Boltzmann function, and observed a clear voltage dependency in its kinetics (Fig. 2 *H*). Aiming to find the effective length, we next varied the length of the linker that connected HaloTag to S1 (Fig. 2 *I*). The linker length had a clear effect (Fig. 2 *J*). With a linker length of 30 residues, the signal was attenuated to nearly one-fourth of that observed with a linker length of five residues. The signal was not detectable with a length of $\geq$60 residues (Fig. 2, *J* and *K*).

Thus, we demonstrated that the structural change in the N-terminal region can also be detected using the TMR-HaloTag reporter at the N-terminus (Fig. 2 *E*). We similarly confirmed a good correlation between the optical signal and gating charge movements (Fig. 3, *A* and *B*). The optical signal from TMR-HaloTag still exhibited slower kinetics than the gating charge movements, but it gave a faster readout compared with the mUKG-mKOκ FRET reporter (Fig. 3 *C*).

Correlated voltage dependencies in the N- and C-terminal effects

D129R eliminated both the N- and C-terminal responses (Fig. 2, *C* and *G*). We also studied the effect of charge

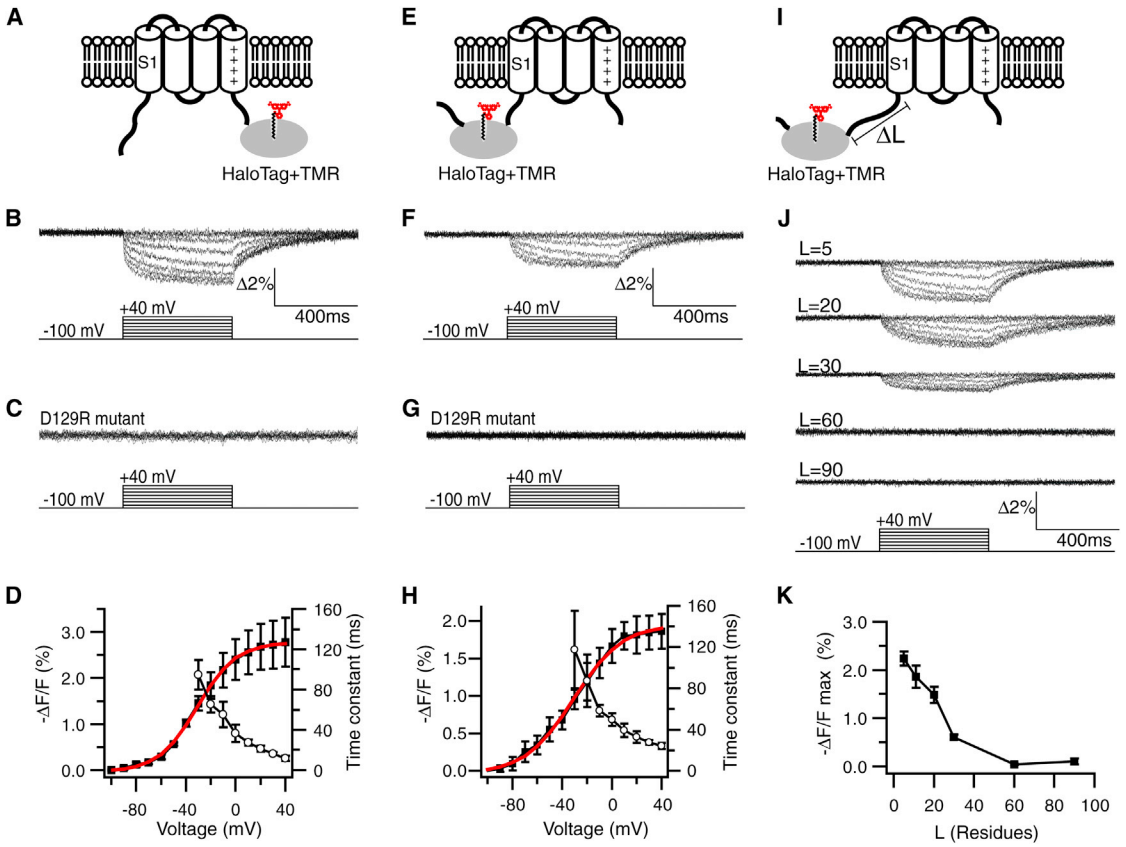

FIGURE 2 Optical signals from a TMR-HaloTag reporter. (*A*) TMR-HaloTag at the C-terminal end of S4. (*B*) TMR signal (ΔF/F) elicited by voltage steps. (*C*) ΔF/F signal from a S4 motion-deficient mutant, D129R. (*D*) Voltage dependence of $-\Delta F/F$ (*solid squares*; *solid line* = single Boltzmann's fit (shown in *red* in the online version), Vmid = −31 mV, Zd = 1.6) and activation kinetics (*open circles*; $n = 4$ cells). (*E*) TMR-HaloTag at the N-terminal end of S1. (*F*) ΔF/F from the construct in *E*. (*G*) ΔF/F from the D129R mutant. (*H*) Voltage dependence of steady-state $-\Delta F/F$ (*solid squares*; *solid line* = fit, Vmid = −31 mV, Zd = 1.4) and its activation kinetics (*open circles*; $n = 7$). (*I*) The length of the HaloTag-S1 linker was varied. (*J*) Representative ΔF/F signals for the indicated linker lengths (L is number of amino acid residues; traces in *F* represent signals for L = 11). (*K*) Plot of $-\Delta F/F_{max}$ [%] versus L ($n = 4$–9 cells). In the online version, the curve fits in *D* and *H* are highlighted in red.

neutralization of the first basic residue in S4 (R217Q). Back mutation to the wild-type form (217R) induced almost identical positive shifts in the voltage dependency of both the C- and N-terminally placed reporters (Fig. 4). These results imply that the N- and C-terminal effects are not independent of one another and likely are triggered by a common voltage-dependent process.

Loading effects on the local rearrangements

We were then interested in whether whole rearrangements of the VSD occur as a rigid fold to exert the N- and C-terminal effects or the nonrigid nature remains. To test this, we studied the effects of HaloTag as a load on local structural rearrangements. We probed local conformational changes using the conventional TMR photometry at two different positions: the top of S4 (G214) (26) and S1 (E144). First, a G214C mutation was introduced and labeled with thiol-reactive TMR-maleimide. HaloTag was left unlabeled and used simply as a load on either S4 (Fig. 5 *A*) or S1 (Fig. 5 *B*). Under the two conditions, the TMR signal showed a nearly identical time course and voltage dependency (Fig. 5, *A–C*), indicating that structural rearrangement around this position is less sensitive to the manner of loading. In contrast, when the E144C mutation was similarly studied, a marked alteration in the TMR signal was noted that depended on the segment loaded (Fig. 5, *D* and *E*). Although stepwise responses were observed in the S4-loaded VSD (Fig. 5 *D*), rapid attenuation was evident in the S1-loaded VSD at higher voltages (Fig. 5 *E*). The voltage dependencies of the maximum fluorescence change were identical irrespective of whether S1 or S4 was loaded, and attenuation was also prominent in the pooled data (Fig. 5 *F*). These results show that the VSD does not transit as a rigid body, but retains a nonrigid nature such that mode of the rearrangements upon transition can be flexibly modulated by adjunctive domains.

DISCUSSION

Since the first molecular identification of the voltage sensor (3), the nature of the VSD has been predominantly

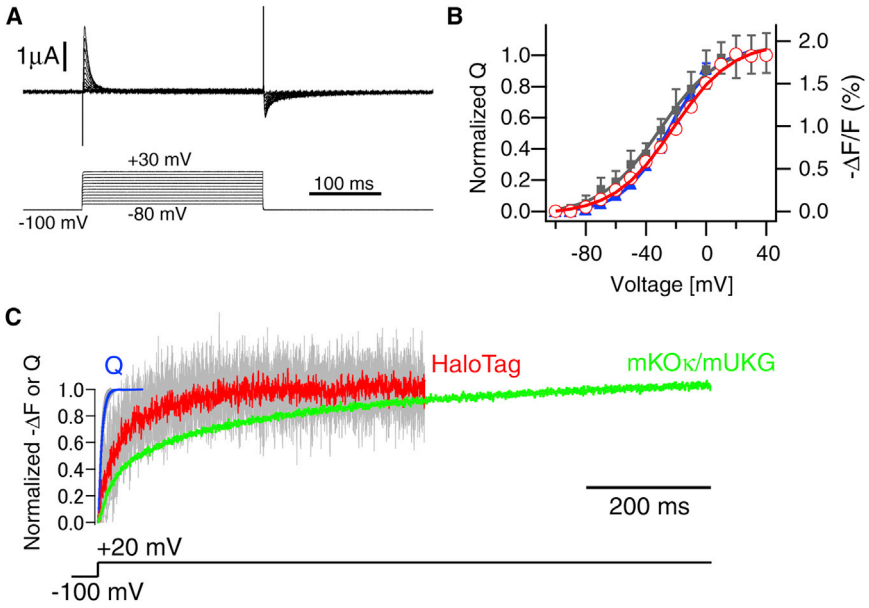

FIGURE 3 Comparison of optical signals from TMR-HaloTag at the N-terminus with gating currents. (*A*) Representative gating currents obtained from a cell expressing the construct shown in Fig. 2 *E*. (*B*) Voltage dependence of on (*solid triangles*; *solid line* = single Boltzmann's fit, Vmid = −25 mV, Zd = 1.6), and off (*open circles*; *solid line* = fit, Vmid = −22 mV, Zd = 1.3) net gating charge movements (n = 4 cells). The voltage dependence of the optical signal (−ΔF/F) is superimposed (*solid square*; data from Fig. 2 *H*). In the online version, the curve fits for Q-on and Q-off are highlighted in blue and red, respectively. (*C*) Comparison of the time course of gating charge movement (Q) and TMR-HaloTag signal in response to voltage step from −100 mV to +20 mV. Responses from four cells and their averages are superimposed. The time course of the FRET response is also presented as a reference (data from Fig. 1 *E*). In the online version, the averaged traces for Q, TMR-HaloTag signal, and FRET signal are highlighted in blue, red, and green, respectively.

investigated with the use of voltage-gated channels. Although the structural modularity of the VSD observed in crystal structures of voltage-gated channels basically reflects its functional independency (4–7), conserved interactions also exist between the VSD and pore that are essential for VSD function (32–34). This implies that the VSDs within voltage-gated channels are evolutionarily adapted to operate properly in the tetrameric fold around the central pore (34). Because the pore also undergoes substantial gating motion, it may be difficult to resolve details of the conformational changes that are intrinsic to the VSD using tetrameric channels. The advantage of the VSP-derived VSD over the channel-based VSD is its tendency to allow robust functional expression in cell membrane alone or as a fusion protein, which is most likely due to its monomeric nature (26). Due to the tractable and robust nature of the VSD derived from monomeric VSP, we were able to functionally introduce two different optical reporters at the N-terminal end of S1, which enabled us to detect optical responses upon VSD transition for the first time (to the best of our knowledge).

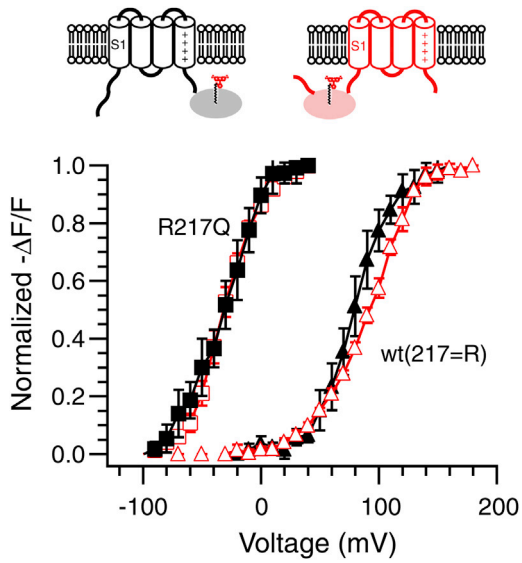

FIGURE 4 Correlated voltage dependencies in optical signals from the N- and C-terminally located reporters. The plot shows the voltage dependence of −ΔF/F signals in the charge-neutralized form (217 = Q; *solid squares* = S4 tagged, n = 4 cells; *open squares* = S1 tagged, n = 7) and the wild-type form (217 = R; *solid triangles* = S4 tagged, n = 4; *open triangles* = S1 tagged, n = 7). In the online version, data for S1-tagged constructs are highlighted in red.

In addition, we showed that local structural rearrangements during transition can be spatially modulated by the manner in which the VSD is loaded, which shows that the motion of the VSD does not always proceed in a spatially consistent manner. Previous studies on channels have also reported flexibility in the VSD motion (e.g., modulation of KCNQ channels by KCNE subunits (35)). However, the direct effect of KCNE subunits on the VSD motion appears to be rather complicated to interpret, because KNCE also has drastic effects on the pore domain (36).

Although this study is based on the VSP-derived VSD, the results may also apply to the channel-derived VSD, considering the functional similarity between them (26). Indeed, the results of some modeling studies suggest that the region upstream of S1 in channels is also less stationary than traditionally thought. These include the KAT1 channel model that was reconstructed using conditional lethal/second-site suppressor screening, which highlights pairs of residues that are in close contact (37), as well as the Shaker channel model that was reconstructed using a combination of cysteine-scanning and voltage-clamp photometry (12).

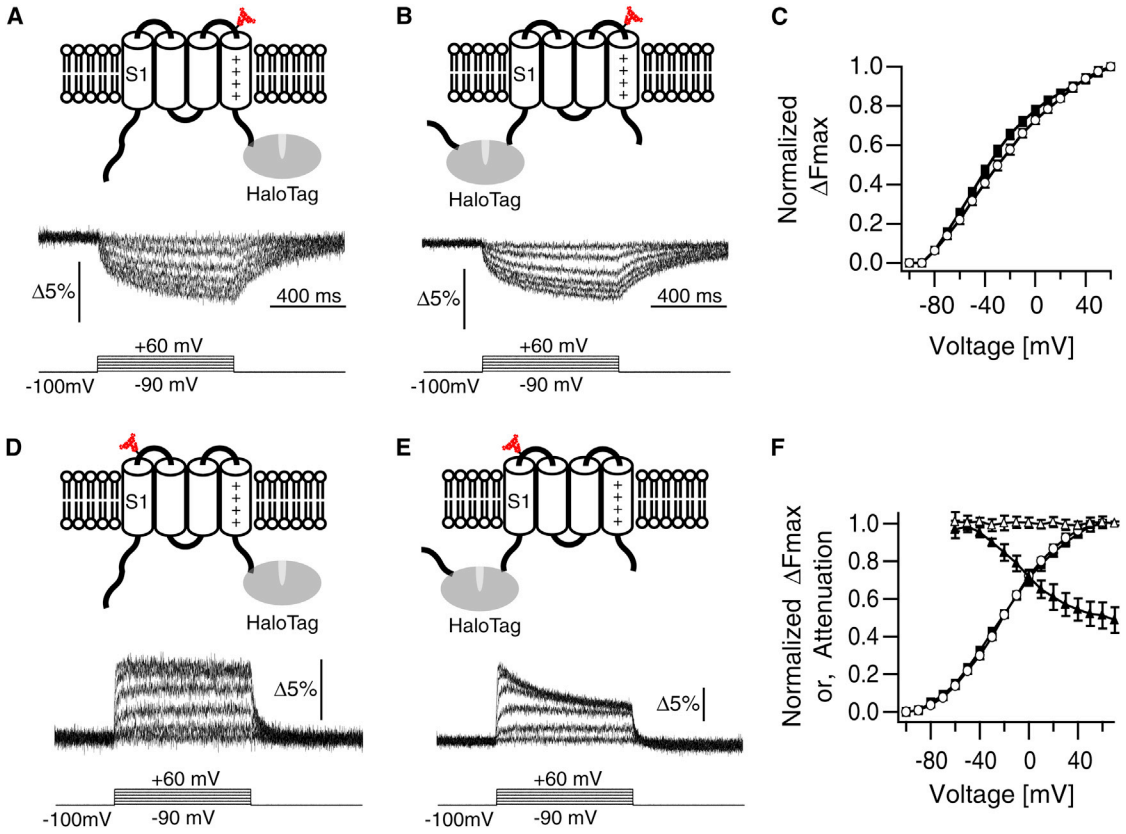

FIGURE 5 Loading effects on the local rearrangements. (*A*) TMR at G214C. S4 is loaded with HaloTag. Representative ΔF/F responses are shown at the bottom. (*B*) TMR at G214C. S1 is loaded with HaloTag. (*C*) Voltage dependence of ΔF_{max} for the construct in *A* (*open circles*, $n = 17$ cells; *solid line* = Boltzmann's fit) and *B* (*solid square*, $n = 6$; *solid line* = Boltzmann's fit). (*D*) TMR at E144C in the S4-loaded VSD. (*E*) TMR at E144C in the S1-loaded VSD. (*F*) Voltage dependence of ΔFmax for the construct in *D* (*open cirlces* = data, $n = 11$; *solid line* = Boltzmann's fit) and *E* (*solid squares* = data, $n = 7$; *solid line* = Boltzmann's fit). Attenuation ($\Delta F_{steady\text{-}state}/\Delta F_{max}$) is plotted versus voltage for the construct in *D* (*open triangles*) and *E* (*solid triangles*).

Although the conclusions from these modeling studies focused mainly on the motions of S4 and the pore, these models also appear to imply the existence of some structural changes in the N-terminus (12,37). However, the approaches are rather indirect, and furthermore, it remains difficult to exclude the possibility that structural changes at the N-terminus only reflect passive displacement induced by the pore motion. Thus, we believe that this study provides the first experimental evidence that directly shows that the S1–S4 segments are sufficient to induce structural effects on the N-terminal region of S1 upon VSD transition.

The most straightforward interpretation of the N-terminal motion would be substantial movement by S1 upon transition. In this case, assuming that the direction of the TMR signal reflects the change in the proximity of the TMR-HaloTag with respect to the membrane, the results obtained using the S1- and S4-tagged constructs (Fig. 2, *B* and *F*) imply that displacement of S1 also involves upward motion, similar to the case with S4. However, other possible scenarios in which other regions (e.g., the S2-S3 loop or the C-terminal tail of S4) somehow directly affect the region N-terminal to S1 cannot be completely excluded.

VSP has a long flanking chain (~100 residues) at its N-terminal end (2). Our results thus imply that in addition to the phosphoinositide signaling regulated by the C-terminal phosphatase domain, the N-terminal region could be involved in distinct voltage-dependent signaling. In voltage-gated channels, S4 motion is considered to be transmitted to the S5-S6 pore segments of the same subunit via the covalent S4-S5 linker to regulate gating (17,18). Under the conventional view that S1-S3(a) is a rather immobile compartment, the intersubunit S1-S5 hydrophobic interaction has been thought to serve as a fulcrum for efficient force transmission (6,14,15). Assuming that S1 in the voltage-gated channel undergoes substantial movement upon transition, as implied in this study, the intersubunit S1-S5 contact may thus act synergistically with the S4-S5 linker to play a more active role in gating. In voltage-gated calcium and sodium channels, the whole tetrameric fold is encoded by a single polypeptide (1). Therefore, force transmission via the interdomain S1-S6 linker may also be also conceivable. Moreover, many voltage-gated channels have been shown to have a variety of physiological functions apart from ion conduction, some of which are also voltage

dependent (38). Therefore, contributions of the N-terminal effect to such nonconducting functions are also conceivable.

CONCLUSIONS

The voltage-induced transition of the VSD is a primary molecular process underlying membrane electrical signaling. In this report, we investigated whether VSD transition induces any structural effects on the N-terminal region of S1. By taking advantage of the VSD derived from monomeric voltage-sensing phosphatase, we studied the behaviors of two different optical reporters placed at the N-terminal end of S1: one based on FRET between a pair of fluorescent proteins and one based on the fluorophore-labeled HaloTag. We found that both reporters were affected upon VSD transition, revealing previously unappreciated features regarding the actions of the VSD. We also observed that whereas the signals from the N- and C-terminally located reporters have rigidly correlated voltage dependencies, the local structural rearrangements reflect the way in which VSD is loaded, demonstrating the flexible nature of the VSD.

SUPPORTING MATERIAL

Two figures and their legends are available at http://www.biophysj.org/biophysj/supplemental/S0006-3495(13)00638-3.

We thank the members of the Laboratory of Integrative Physiology for comments and discussions. We are also grateful to Dr. Eamonn Dickson for valuable comments.

This work was supported by grants from JST-PRESTO (H.T.), MEXT (H.T. and Y.O.), and HFSP (Y.O.).

REFERENCES

1. Hille, B. 2001. Ion Channels of Excitable Membranes. Sinauer, MA.
2. Murata, Y., H. Iwasaki, …, Y. Okamura. 2005. Phosphoinositide phosphatase activity coupled to an intrinsic voltage sensor. *Nature.* 435:1239–1243.
3. Noda, M., T. Ikeda, …, S. Numa. 1986. Expression of functional sodium channels from cloned cDNA. *Nature.* 322:826–828.
4. Jiang, Y., A. Lee, …, R. MacKinnon. 2003. X-ray structure of a voltage-dependent K+ channel. *Nature.* 423:33–41.
5. Long, S. B., E. B. Campbell, and R. Mackinnon. 2005. Crystal structure of a mammalian voltage-dependent Shaker family K+ channel. *Science.* 309:897–903.
6. Long, S. B., X. Tao, …, R. MacKinnon. 2007. Atomic structure of a voltage-dependent K+ channel in a lipid membrane-like environment. *Nature.* 450:376–382.
7. Payandeh, J., T. Scheuer, …, W. A. Catterall. 2011. The crystal structure of a voltage-gated sodium channel. *Nature.* 475:353–358.
8. Chanda, B., O. K. Asamoah, …, F. Bezanilla. 2005. Gating charge displacement in voltage-gated ion channels involves limited transmembrane movement. *Nature.* 436:852–856.
9. Milescu, M., J. Vobecky, …, K. J. Swartz. 2007. Tarantula toxins interact with voltage sensors within lipid membranes. *J. Gen. Physiol.* 130:497–511.
10. Ruta, V., J. Chen, and R. MacKinnon. 2005. Calibrated measurement of gating-charge arginine displacement in the KvAP voltage-dependent K+ channel. *Cell.* 123:463–475.
11. Yang, N., and R. Horn. 1995. Evidence for voltage-dependent S4 movement in sodium channels. *Neuron.* 15:213–218.
12. Pathak, M. M., V. Yarov-Yarovoy, …, E. Y. Isacoff. 2007. Closing in on the resting state of the Shaker K(+) channel. *Neuron.* 56:124–140.
13. Glauner, K. S., L. M. Mannuzzu, …, E. Y. Isacoff. 1999. Spectroscopic mapping of voltage sensor movement in the Shaker potassium channel. *Nature.* 402:813–817.
14. Cha, A., G. E. Snyder, …, F. Bezanilla. 1999. Atomic scale movement of the voltage-sensing region in a potassium channel measured via spectroscopy. *Nature.* 402:809–813.
15. Swartz, K. J. 2008. Sensing voltage across lipid membranes. *Nature.* 456:891–897.
16. Catterall, W. A. 2010. Ion channel voltage sensors: structure, function, and pathophysiology. *Neuron.* 67:915–928.
17. Jiang, Y., V. Ruta, …, R. MacKinnon. 2003. The principle of gating charge movement in a voltage-dependent K+ channel. *Nature.* 423:42–48.
18. Lu, Z., A. M. Klem, and Y. Ramu. 2002. Coupling between voltage sensors and activation gate in voltage-gated K+ channels. *J. Gen. Physiol.* 120:663–676.
19. Lu, Z., A. M. Klem, and Y. Ramu. 2001. Ion conduction pore is conserved among potassium channels. *Nature.* 413:809–813.
20. Dimitrov, D., Y. He, …, T. Knöpfel. 2007. Engineering and characterization of an enhanced fluorescent protein voltage sensor. *PLoS ONE.* 2:e440.
21. Tsutsui, H., S. Karasawa, …, A. Miyawaki. 2008. Improving membrane voltage measurements using FRET with new fluorescent proteins. *Nat. Methods.* 5:683–685.
22. Sawano, A., and A. Miyawaki. 2000. Directed evolution of green fluorescent protein by a new versatile PCR strategy for site-directed and semi-random mutagenesis. *Nucleic Acids Res.* 28:E78.
23. Murata, Y., and Y. Okamura. 2007. Depolarization activates the phosphoinositide phosphatase Ci-VSP, as detected in Xenopus oocytes coexpressing sensors of PIP2. *J. Physiol.* 583:875–889.
24. Goldin, A. L. 1992. Maintenance of Xenopus laevis and oocyte injection. *Methods Enzymol.* 207:266–279.
25. Mannuzzu, L. M., M. M. Moronne, and E. Y. Isacoff. 1996. Direct physical measure of conformational rearrangement underlying potassium channel gating. *Science.* 271:213–216.
26. Kohout, S. C., M. H. Ulbrich, …, E. Y. Isacoff. 2008. Subunit organization and functional transitions in Ci-VSP. *Nat. Struct. Mol. Biol.* 15:106–108.
27. Lakowicz, J. R. 2006. Principles of Fluorescence Spectroscopy. Springer, NY.
28. Gandhi, C. S., E. Loots, and E. Y. Isacoff. 2000. Reconstructing voltage sensor-pore interaction from a fluorescence scan of a voltage-gated K+ channel. *Neuron.* 27:585–595.
29. Ohana, R. F., L. P. Encell, …, K. V. Wood. 2009. HaloTag7: a genetically engineered tag that enhances bacterial expression of soluble proteins and improves protein purification. *Protein Expr. Purif.* 68:110–120.
30. Encell, L. P., R. Friedman Ohana, …, K. V. Wood. 2012. Development of a dehalogenase-based protein fusion tag capable of rapid, selective and covalent attachment to customizable ligands. *Curr. Chem. Genomics.* 6:55–71.
31. Tsutsui, H., S. Higashijima, …, Y. Okamura. 2010. Visualizing voltage dynamics in zebrafish heart. *J. Physiol.* 588:2017–2021.
32. Broomand, A., R. Männikkö, …, F. Elinder. 2003. Molecular movement of the voltage sensor in a K channel. *J. Gen. Physiol.* 122:741–748.

33. Gandhi, C. S., E. Clark, …, E. Y. Isacoff. 2003. The orientation and molecular movement of a k(+) channel voltage-sensing domain. *Neuron.* 40:515–525.

34. Lee, S. Y., A. Banerjee, and R. MacKinnon. 2009. Two separate interfaces between the voltage sensor and pore are required for the function of voltage-dependent K(+) channels. *PLoS Biol.* 7:e47.

35. Osteen, J. D., C. Gonzalez, …, R. S. Kass. 2010. KCNE1 alters the voltage sensor movements necessary to open the KCNQ1 channel gate. *Proc. Natl. Acad. Sci. USA.* 107:22710–22715.

36. Nakajo, K., and Y. Kubo. 2011. Nano-environmental changes by KCNE proteins modify KCNQ channel function. *Channels (Austin).* 5:397–401.

37. Grabe, M., H. C. Lai, …, L. Y. Jan. 2007. Structure prediction for the down state of a potassium channel voltage sensor. *Nature.* 445:550–553.

38. Kaczmarek, L. K. 2006. Non-conducting functions of voltage-gated ion channels. *Nat. Rev. Neurosci.* 7:761–771.